# Modifications of Alamethicin Ion Channels by Substitution of Glu-7 for Gln-7

Koji Asami,* Takashi Okazaki,* Yasuaki Nagai,* and Yasuo Nagaoka†
*Institute for Chemical Research, Kyoto University, Uji, Kyoto 611-0011, Japan; and †Faculty of Pharmaceutical Science, Kyoto University, Sakyo-ku, Kyoto 606-0001, Japan

ABSTRACT To evaluate the role of charged residues facing a pore lumen in stability of channel structure and ion permeation, we studied electrical properties of ion channels formed by synthesized native alamethicins (Rf50 (alm-Q7Q18) and Rf30 (alm-Q7E18)) and their analogs with Glu-7 (alm-E7Q18 and alm-E7E18). The single-channel currents were measured over a pH range of 3.5 to 8.7 using planar bilayers of diphytanoyl PC. The peptides all showed multi-level current fluctuations in this pH range. At pH 3.5 the channels formed by the four peptides were similar to each other irrespective of the side chain differences at positions 7 and 18. The ionization of Glu-7 (E7) and Glu-18 (E18) above neutral pH reduced the relative probabilities of low-conductance states (levels 1 and 2) and increased those of high-conductance states (levels 4–6). The channel conductance of the peptides with E7 and/or E18, which was distinct from that of alm-Q7Q18, showed a marked pH-dependence, especially for low-conductance states. The ionization of E7 further reduced the stability of channel structure, altered the current-voltage curve from a superlinear relation to a sublinear one, and enhanced cation selectivity. These results indicate that ionized E7 strongly influences the channel structure and the ion permeation, in contrast to ionized E18.

## INTRODUCTION

Alamethicin isolated from *Trichoderma viride* is a mixture of 20-residue amphipathic peptides with eight $\alpha$-aminoisobutyric acids (Aib) and a phenylalaninol at the C-terminus. The major components are called Rf50 and Rf30, which differ only in whether residue 18 is either Gln or Glu. Both Rf50 and Rf30 form voltage-gated ion channels in bilayer lipid membranes, which have been extensively studied (for reviews, Latorre and Alvarez, 1981; Woolley and Wallace, 1992; Sansom, 1991, 1993; Cafiso, 1994). In the ion channels, peptide helices are supposed to be packed together in parallel around a central ion permeable pore. This channel structure, called the "helix-bundle" model or the "barrel-stave" model (Baumann and Mueller, 1974; Boheim, 1974), resembles a structural motif of pore regions in some biological ion channels such as nAChR, and therefore alamethicin provides a simple model system for exploring structure-function relationships in ion channels. In the alamethicin ion channels, hydrophilic residues, Gln-7 and Glu-18 (or Gln-18), face the pore lumen and probably form hydrogen-bonded rings, being expected to play a key role in the channel stability and the ion permeation (Fox and Richards, 1982). In particular, Gln-7 located at the narrowest part of the pore might be more important.

To examine this idea, functional modifications of alamethicin channels have been studied by replacing Gln-7 and Gln-18 by other amino acid residues. Gln-7 was replaced by Ala in Rf30 (Kaduk et al., 1998); by Ala, Asn, or Ser in synthetic des-Aib alamethicin analogs in which all Aib residues are replaced by Leu (Molle et al., 1996); and by Ala in trichosporin-B-Via, having a sequence similar to alamethicin (Nagaoka et al., 1996a). These modifications did not diminish channel-forming activity except for the replacement of Gln-7 by Ala in des-Aib alamethicin analogs, but reduced the lifetime of channel opening and changed the channel conductance. The replacement of Gln-18 by Lys in covalent dimers of alamethicin altered the charge selectivity of ion permeation from weakly cation-selective to weakly anion-selective at neutral pH (Starostin et al., 1999; Borisenko et al., 2000).

In this paper we have studied the effects of the replacement of Gln-7 by Glu-7 in Rf50 and Rf30 on channel formation and ion permeation. Four peptides, Rf50 (alm-Q7Q18), Rf30 (alm-Q7E18), alm-E7Q18, and alm-E7E18 (see Table 1) were synthesized by a solid-phase method and their single-channel recordings were carried out using planar bilayer lipid membranes. Because our main concern was to reveal the effects of the ionization of Glu-7 and Glu-18 on channel properties, the pH of the membrane-bathing solutions was varied from 3.5 to 8.7.

## MATERIALS AND METHODS

### Peptide synthesis

The peptides whose sequences are shown in Table 1 were synthesized by the solid-phase method with Fmoc-amino acid fluorides described by Wenschuh et al. (1995). The solid support used was an *o*-chlorotrityl resin, to which the C-terminal phenylalaninol, Pheol, was directly anchored. To assemble sterically hindered $\alpha$-aminoisobutyric acid (Aib) and amino acids next to Aib, their Fmoc-amino acid fluorides were used as coupling agents, which were prepared from the Fmoc-amino acids using cyanuryl fluoride (Bertho et al., 1991). The other amino acids were assembled by the

*Submitted October 18, 2001, and accepted for publication March 6, 2002.*

Address reprint requests to Dr. Koji Asami, Institute for Chemical Research, Kyoto University, Uji, Kyoto 611-0011, Japan. Tel.: +81-774-38-3081; Fax: +81-774-38-3084; E-mail: asami@tampopo.kuicr.kyoto-u.ac.jp.

Y. Nagaoka's current address is Department of Biotechnology, Kansai University, Suita, Osaka 564-8680, Japan.



0006-3495/02/07/219/10 $2.00

**TABLE 1 Amino acid sequences of alamethicins and their analogs**

| Peptides | 1 | 7 | 18 | 20 |
|---|---|---|---|---|
| alm-Q7Q18 (Rf50) | Ac-U-P-U-A-U-A-Q-U-V-U-G-L-U-P-V-U-U-Q-Q-Pheol | | | |
| alm-Q7E18 (Rf30) | | Q | E | |
| alm-E7Q18 | | E | Q | |
| alm-E7E18 | | E | E | |

Ac, acetyl; U, $\alpha$-aminoisobutyric acid; Pheol, phenylalaninol.

standard method with Fmoc-amino acids. After completion of the assemblage followed by acetylation of the N-terminus, the peptides were cleaved from the resin. The peptides were purified through a column of Sephadex LH-20 (Amersham Bioscience, Uppsala, Sweden) with methanol and then by reverse-phase HPLC on a YMC-ODS column (YMC, Kyoto, Japan) with elutes containing 63–68% $CH_3CN$, 37–32% $H_2O$, and 0.05% TFA. The HPLC chromatograms of the purified peptides showed single peaks whose retention times at 40°C were 33 min for alm-Q7Q18 (with a $CH_3CN/H_2O$ ratio of 63:37), 29 min for alm-Q7E18 (65:35), 29 min for alm-E7Q18 (65:35) and 31 min for alm-E7E18 (68:32). The purified peptides were characterized by ESI-MS with an API-3000 (Perkin-Elmer Sciex, Wellesley, MA) as follows: m/z 982.2 $[M+2H^+]$ and 655.1 $[M+3H^+]$ for alm-Q7Q18 (MW = 1962.4); m/z 982.7 $[M+2H^+]$ and 655.4 $[M+3H^+]$ for alm-Q7E18 (MW = 1963.3); m/z 983.0 $[M+2H^+]$ and 656.0 $[M+3H^+]$ for alm-E7Q18 (MW = 1963.3); m/z 983.2 $[M+2H^+]$ for alm-E7E18 (MW = 1964.3). Fig. 1 show the ESI-MS charts and the HPLC traces of purified alm-E7Q18 and alm-E7E18, indicating that those are of adequate purity. Similar ESI-MS charts and HPLC traces were obtained for alm-E7Q18 and alm-E7E18 (not shown).

## Single-channel measurement

Single ion channel recordings were performed with planar bilayer lipid membranes prepared by the monolayer-folding technique (Montal and Mueller, 1972), as described in previous papers (Nagaoka et al., 1996b; Koide et al., 1997). Lipid membranes were formed from diphytanoyl phosphatidyl choline (diphy-PC) (Avanti Polar Lipids, Alabaster, AL) in 1 M KCl buffered with 10 mM MES-KOH (pH 3.5, 4.7, 5.9), 10 mM HEPES-KOH (pH 6.7–7.0), or 10 mM TRIS-HCl (pH 8.3–8.7). Small amounts of a peptide solution in ethanol were added only to one side of a membrane (*cis* side) to give a final concentration of 1–10 nM.

A pair of Ag-AgCl electrodes was used for current measurement and voltage supply. The *cis*- and *trans*-side electrodes were connected to a DC voltage source and to the virtual ground of a homemade current amplifier, respectively. Hence, a positive voltage means that the *cis* side is positive relative to the *trans* side. The output voltages of the current amplifier were recorded with a DR-F2a digital recorder (TEAC Corporation, Tokyo, Japan). All measurements were performed at 25 ± 0.5°C.

In the single-channel recordings we carefully adjusted applied voltage not to count plural channels per membrane. The critical applied voltage depended on peptide concentration in the bathing solution, and therefore voltage dependence of single-channel currents was obtained by varying peptide concentration. Relative probabilities of different conductance states were calculated from the single-channel recordings, being almost independent of either peptide concentration or applied voltage.

Ion selectivity of single channels between $K^+$ and $Cl^-$ was measured with solutions of potassium and chloride salts with bulky counterions that negligibly contribute to the channel current. This method was the same as described by Starostin et al. (1999). The electrolyte solutions used were 1 M potassium gluconate (Kgluc) (Wako Pure Chemical Industries, Osaka, Japan) and 1 M *N*-methylglucamine chloride (NmgCl) (Tokyo Kasei Kogyo, Tokyo, Japan) both containing 10 mM HEPES-KOH (pH 7.0). The conductances of the Kgluc and NmgCl solutions measured using a HP-4192A LF Impedance Analyzer (Hewlett-Packard, Palo Alto, CA), were close to each other, 39% and 38% of that of 1 M KCl with 10 mM HEPES-KOH (pH 7.0), respectively.

## Theoretical calculation of single-channel current

Single-channel currents in symmetric KCl solutions were calculated by a method similar to that described by Dieckmann et al. (1999). In their method, the Nernst-Planck equation was used with potential energy profiles for permeating ions in a pore, which were calculated with a macroscopic pore model by a three-dimensional finite-differential Poisson-Boltzmann (FDPB) method (Sharp and Honig, 1990). In this study, to save time

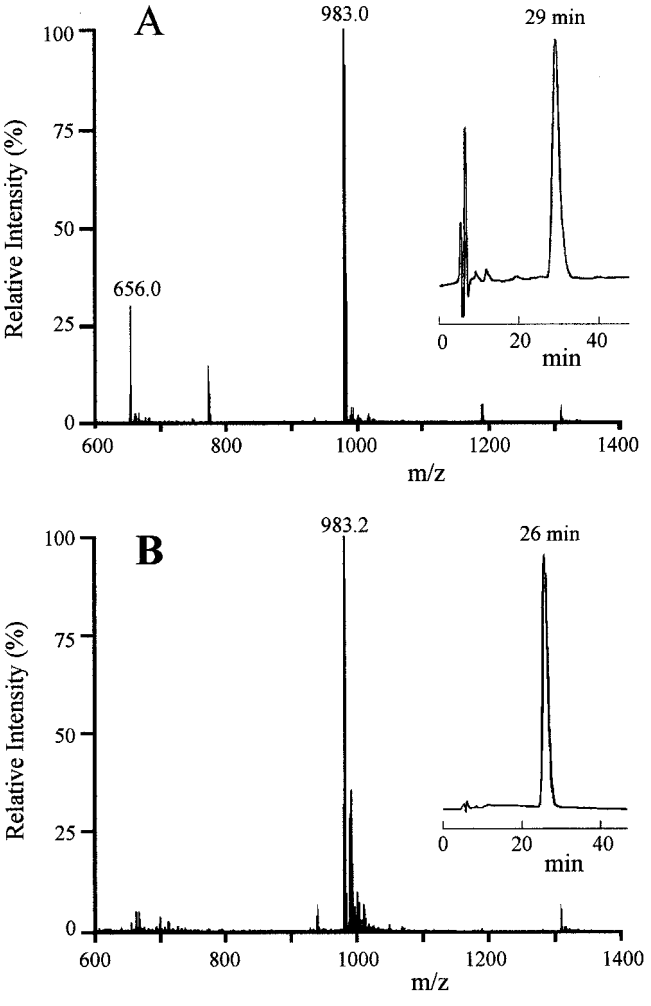


FIGURE 1 ESI-MS charts of (*A*) alm-E7Q18 and (*B*) alm-E7E18. *Inset:* HPLC chromatographs.

in FDPB calculation, we adopted an axial symmetric geometry (Jordan et al., 1989). The grid dimensions were 65 (radial) × 75 (axial) whose radial and axial grid spacing were 0.05 nm and 0.125 nm, respectively. The electrostatic potential energy for a permeating ion is provided by a sum of the "desolvation" (or image) energy and the "interaction" energy. The "desolvation" energy is the self energy difference due to interactions between a probe ion and charges induced at boundaries between different dielectrics (Parsegian, 1969). The "interaction" energy comes from the interactions of a permeating ion with charges of ionized residues and dipole moments of helix backbones.

In the calculation with the Nernst-Planck equation, we assumed that a transmembrane voltage $V$ produces a constant electric field in the pore. Because both the *cis* and *trans* sides have the same KCl solution of activity, $a_{KCl}$, the single-channel current $I$ is simply given by

$$I = \frac{\pi r^2 F a_{KCl}}{d}\left(D_K \frac{\exp(VF/RT) - 1}{S_K} - D_{Cl}\frac{\exp(-VF/RT) - 1}{S_{Cl}}\right), \quad (1)$$

$$S_K = \frac{1}{d}\int_0^d \exp\left(\frac{V(1 - x/d)F}{RT} + \frac{\Phi_K}{RT}\right)dx, \quad (2)$$

$$S_{Cl} = \frac{1}{d}\int_0^d \exp\left(-\frac{V(1 - x/d)F}{RT} + \frac{\Phi_{Cl}}{RT}\right)dx, \quad (3)$$

where $d$ is the pore length, $r$ the pore radius, $\Phi$ the electrostatic potential energy of a permeating ion, $D$ the ion diffusion coefficient, $F$ the Faraday constant, and subscripts K and Cl refer to $K^+$ and $Cl^-$ ions, respectively.

## RESULTS AND DISCUSSION

### Single-channel recordings

Single ion channel currents were measured for ion channels formed in diphy-PC bilayers by two native alamethicins Rf50 (alm-Q7Q18) and Rf30 (alm-Q7E18) and their analogs with Glu-7 (E7) instead of Gln-7 (Q7) (alm-E7Q18 and alm-E7E18). The effects of the ionization of E7 and E18 on the ion channel properties were examined by varying pH of the membrane-bathing solutions (1 M KCl) from 3.5 to 8.7. In this pH range the headgroup of diphy-PC is electrically neutral and the contributions of $H^+$ and $OH^-$ to the channel currents are negligible. When the peptides were added to one side (*cis* side) of the membrane, multi-level current fluctuations were observed only at *cis*-positive voltages. Fig. 2 shows typical examples of current fluctuations measured at 200 mV and at pH 3.5, 6.7–6.9, and 8.3–8.7. The corresponding conductance histograms (all-point amplitude histograms) are shown in Fig. 3. The current fluctuations of alm-Q7Q18 channels were almost independent of pH, and four conductance states (levels 1–4) were found besides the lowest conductance state (level 0) (Hanke and Boheim, 1980) that was not properly resolved from the closed state in the histograms. The relative probabilities of the conductance states decreased with increasing conductance-level number. Very similar behavior was found with alm-Q7E18, alm-E7Q18, and alm-E7E18 at pH 3.5, where E7 and E18 were not ionized. This suggests that, when E residues are not ionized, the channels of the four peptides are similar to each other in structure and stability, irrespective of the side chain differences.

For the peptides with E7 and/or E18 at pH 6.7–6.9 and pH 8.3–8.7, the relative probabilities of low-conductance states (levels 1 and 2) decreased significantly, and those of high-conductance states (levels 4–6) increased. The conductance histograms were "bell-shaped," in which the major conductance state was level 4 for alm-Q7E18, level 4–5 for alm-E7Q18, and level 5–6 for alm-E7E18. This indicates that the ionization of E7 and/or E18 inhibits formation of smaller pores and facilitates that of larger pores, which might be due to electrostatic repulsion between peptides in a channel. The relative probabilities of conductance states may be determined by peptide/peptide and peptide/lipid interactions. The importance of peptide/lipid interactions has been clearly demonstrated by Keller et al. (1993) and Bezrukov et al. (1998), i.e., lipid packing stress promoted higher conductance states. The present findings show that peptide/peptide interactions are also an important factor that governs the relative probabilities of conductance levels.

The peptides with E7 (alm-E7Q18 and alm-E7E18) at pH 6.7–6.9 and pH 8.3–8.7 showed rapid transitions between adjacent conductance states in the current fluctuations and broadening and splitting of peaks in the conductance histograms. This behavior implies that the ionization of E7 residues at the narrowest part of the pore destabilizes the channel structure and produces different conformations, in contrast to ionized E18 residues near the pore mouth.

The molecularity of alamethicin per channel in each conductance state has been discussed by several authors (Hanke and Boheim, 1980; Sansom, 1991; Matsubara et al., 1996; You et al., 1996). Because the transitions between adjacent conductance states may be caused by the uptake and release of a peptide from a helix bundle, the number of peptides per channel increases one by one with increasing conductance-level number. Hanke and Boheim (1980) suggested that the lowest-conductance channel (termed level 0 channel in this paper) is a trimeric bundle following macroscopic calculations with a cylindrical model. Matsubara et al. (1996) supported this assignment by using alamethicin molecules tethered with cyclic templates. Their conclusion, however, should be reconsidered because the cyclic templates are liable to interfere with normal packing of helices in a channel. You et al. (1996) compared the conductance levels between the alamethicin monomer and its covalent dimer, suggesting that the number of peptides in level 0, 2, and 4 channels (or level 1, 3, and 5 channels in their notation) is an even number, putatively 4, 5, 6, 7, and 8 for levels 0, 1, 2, 3, and 4, respectively. Our similar studies with N-terminally linked dimers by a disulfide bond have also

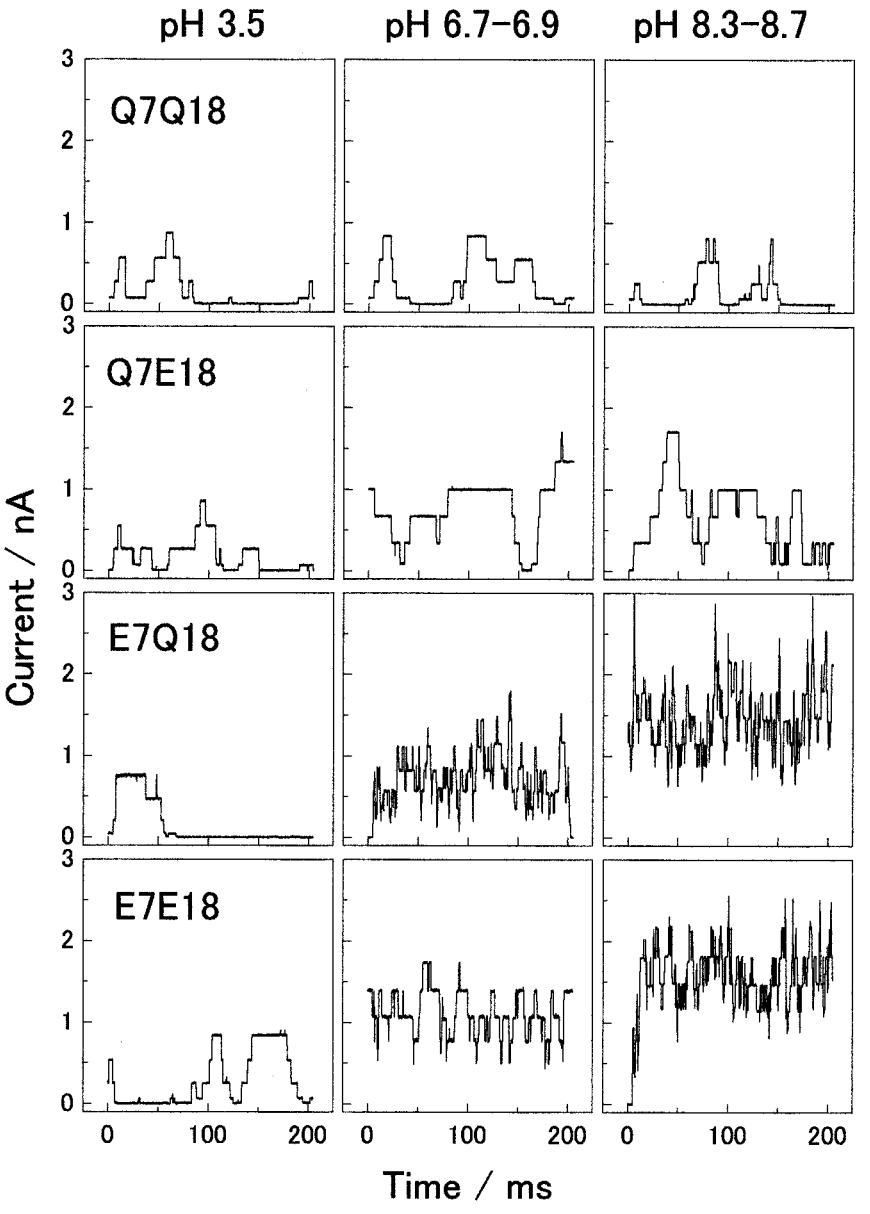


FIGURE 2 Typical current recordings of single ion channels formed in diphy-PC bilayer membranes by alm-Q7Q18 (*first row*), alm-Q7E18 (*second row*), alm-E7Q18 (*third row*), and alm-E7E18 (*fourth row*). The data were obtained at pH 3.5 (*left column*), 6.7–6.9 (*middle column*), and 8.3–8.7 (*right column*). The membrane-bathing solutions, buffered 1 M KCl; applied voltage, 200 mV; temperature, 25°C.

supported their conclusion (a preliminary report was presented at the 39th annual meeting of the Biophysical Society of Japan, 2001).

## pH-dependence of channel conductance

Fig. 4 shows pH-dependence of the conductance of level 2 channels that were commonly observed for all the peptides over the pH range examined. The channel conductance of alm-Q7Q18 was almost independent of pH. The conductance of the alm-Q7E18 channel increased with pH from 3.5 to 6 and leveled off above pH 6, whereas that of the alm-E7Q18 channel started to increase at pH 5 and still increased above pH 6. The conductance of alm-E7E18 channel appeared to be a sum of the contributions of ionized E7 and E18 that were obtained with alm-E7Q18 and alm-Q7E18, respectively. The influence of pH on the channel conductance decreased with increasing conductance-level number (see Fig. 3).

The pH-dependence of channel conductance is related to the dissociation of E residues, which is influenced by their surroundings such as electrolyte shielding and ionized states of their neighbors. The effective $pK_a$ value that was estimated to be 4.5–5 from the pH-dependence of channel conductance for alm-Q7E18 was close to that of free E residues, indicating small electrostatic interactions between E18 residues in a channel. The change in channel conductance for alm-E7Q18, which was distinct from alm-Q7E18, spread over a wider pH region, suggesting electrostatic interactions between E7 residues in a channel alter the

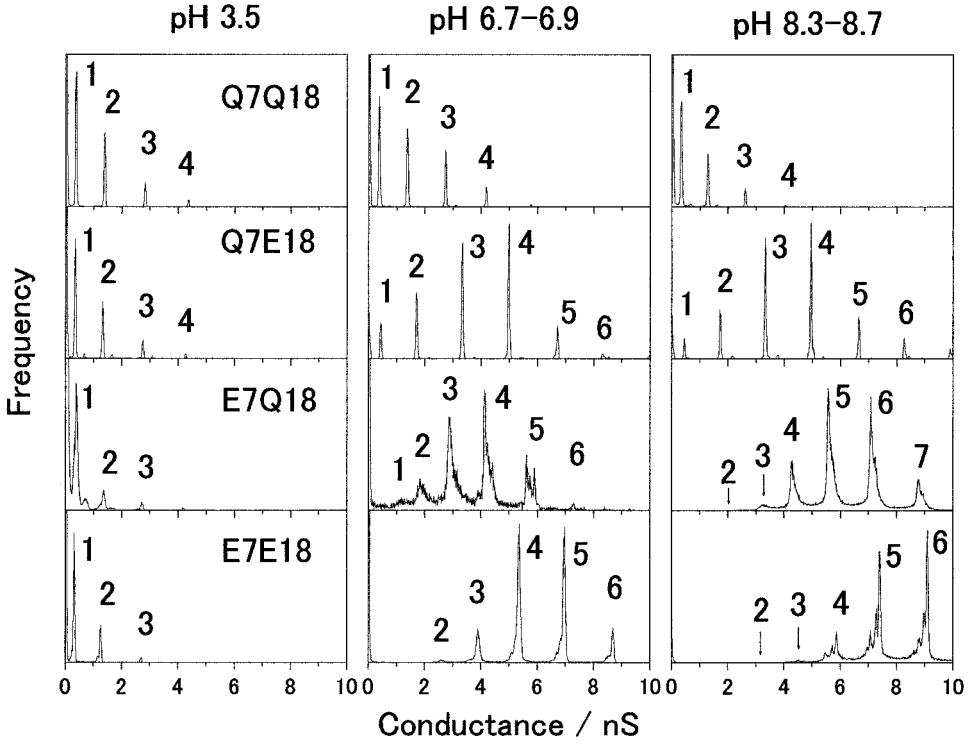


FIGURE 3 Conductance histograms for channels of alm-Q7Q18 (*first row*), alm-Q7E18 (*second row*), alm-E7Q18 (*third row*), and alm-E7E18 (*fourth row*) obtained from their current recordings (Fig. 2). The data were obtained at pH 3.5 (*left column*), 6.7–6.9 (*middle column*), and 8.3–8.7 (*right column*). The figures beside the peaks indicate conductance-level numbers.

effective $pK_a$ values. Borisenko et al. (2000) calculated the effective $pK_a$ values of eight Lys residues in an octameric bundle. The results showed that the effective $pK_a$ was considerably shifted to a lower value with increasing the number of ionized Lys residues. For acidic residues, the reverse change in $pK_a$ is expected, explaining the broad pH-dependence of channel conductance for alm-E7Q18 and alm-E7E18. The electrostatic interactions between adjacent E residues depend on their positions in the pore. The E7 residues located at the narrowest part of the pore are closer to each other and are less subjected to electrolyte shielding effects than the E18 residues near the pore mouth. This might explain the difference in pH-dependence of channel conductance between alm-Q7E18 and alm-E7Q18.

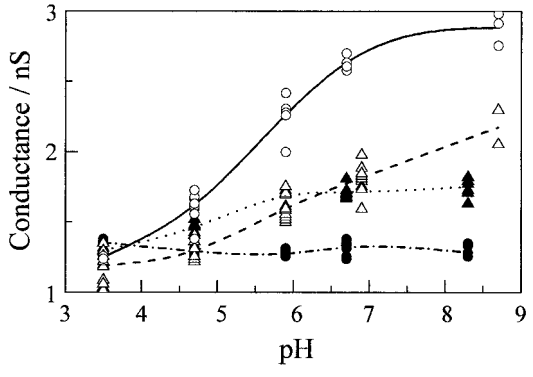


FIGURE 4 pH-dependence of conductance of level 2 channels measured at 200 mV for alm-Q7Q18 (*solid circle*), alm-Q7E18 (*solid triangle*), alm-E7Q18 (*open triangle*), and alm-E7E18 (*open circle*). Mean values were connected by dot-dashed (alm-Q7Q8), dotted (alm-Q7E18), broken (alm-E7Q18), and solid (alm-E7E18) lines.

## Single-channel current-voltage relationships

Non-ohmic behavior of single channels has been reported for alamethicin (Eisenberg et al., 1973; Gordon and Haydon, 1975; Taylor and de Levie, 1991) and for covalent dimers of alamethicin (Woolley and Wallace, 1992), providing insights into energy barrier profiles for the ion permeation. Fig. 5 shows the *I-V* relationships of the single channels obtained for the four peptides at pH 7.0. To compare the *I-V* curves among different conductance levels, those were normalized with current values at 200 mV. The normalized *I-V* curves of alm-Q7Q18 and alm-Q7E18 channels were similar to each other and changed from a superlinear (concave) relation to a linear one with increasing conductance-level number. These *I-V* curves were well represented by a hyperbolic sine function as described previously (Mak and Webb, 1995; Koide et al., 1997). Similar

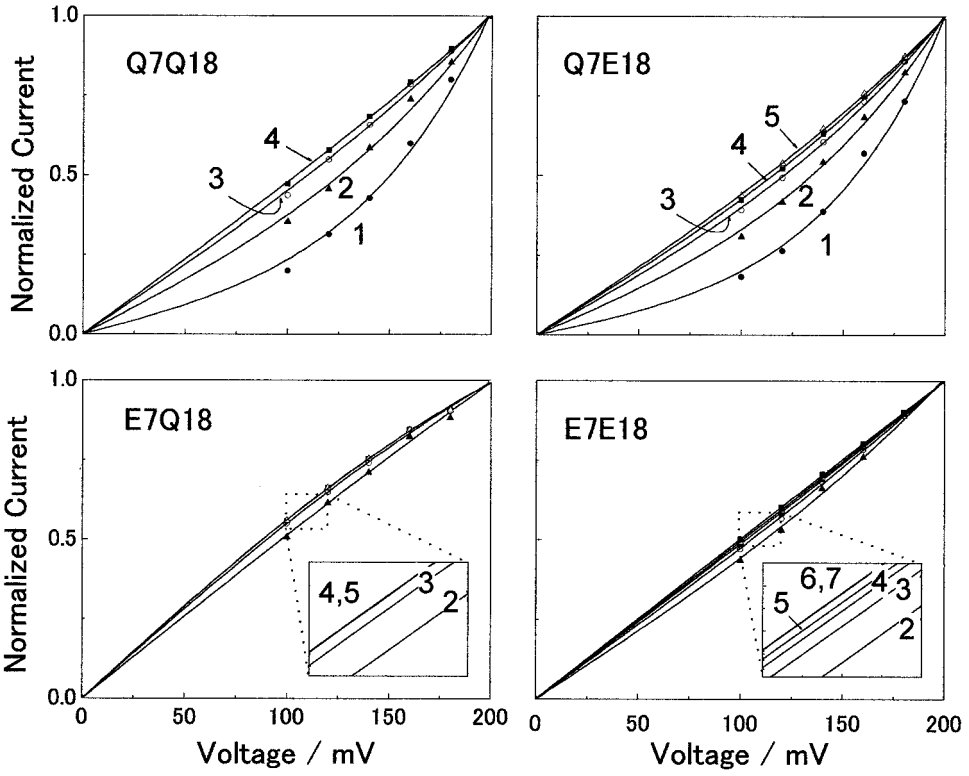


FIGURE 5 Normalized current-voltage relationships for single channels of alm-Q7Q18, alm-Q7E18, alm-E7Q18, and alm-E7E18 at pH 6.7–6.9. The solid lines are obtained by fitting a hyperbolic sine function to the data of Q7Q18, Q7E18, and E7E18 (levels 1- 5) and by fitting a hyperbolic tangent function to the data of E7Q18 and E7E18 (levels 6 and 7). The figures beside the curves indicate conductance-level numbers.

*I-V* curves were also obtained for alm-E7Q18 and alm-E7E18 at pH 3.5 (not shown).

The *I-V* curves of alm-E7Q18 channels at pH 7.0 showed slightly sublinear (convex) relations. The degree of deviation from a linear relation increased with conductance-level number. The channels of alm-E7E18 showed slightly superlinear curves at levels 2–4, a linear one at level 5, and slightly sublinear ones for level 6–7. The results indicated that the ionization of E7 converted the *I-V* curve from a superlinear relation to a sublinear one, whereas the ionization of E18 little influenced the shape of *I-V* curves.

The effects of charged E residues on the *I-V* relationships depended on their positions in a pore. Here, we attempt to simulate the effects for the level 2 channels of the four peptides at pH 6.7–6.9. The precise simulations are, however, not easy at present because of the following reasons: 1) we don't yet have the precise molecular model of alamethicin channels in lipid bilayers under electric fields, and 2) the method for calculating ion flux from a molecular pore model is still controversial (Levitt, 1999). Hence, we intended to provide rather a rough explanation following the line described by Dieckmann et al. (1999). The *I-V* curves were calculated by the Nernst-Planck equation from the potential energy profiles for a permeating ion that were estimated using macroscopic pore models.

Three pore models were examined, which have different electrolyte-occupied regions: electrolytes are excluded from the pore (model A), and penetrate the pore entrances (model B) and the entire pore interior (model C) (Fig. 6). The pore shape in the models were similar to that obtained by Tieleman et al. (1999) for a hexameric bundle of alm-Q7Q18 and alm-Q7E18 using molecular dynamics simulations. The relative permittivity of the aqueous phase including the pore interior was assumed to be 80, and that of the membrane and the pore wall to be 2. The membrane thickness was 3.5 nm. For the sake of simplicity we dealt with only the charges of ionized groups and the macro dipoles due to the peptide helix backbones (the dipole moment is $2.4 \times 10^{-28}$ Cm per peptide helix). The potential energy profiles for a permeating ion along the pore axis were calculated by a nonlinear FDPB method, from which single-channel currents were calculated using the Nernst-Planck equation with the following parameter values: $D_K = D_{Cl} = 1.9 \times 10^{-9}$ m$^2$/s (the value is for bulk KCl solutions), $a_{KCl} = 0.6$ M for 1 M KCl, $d = 3.5$ nm, and $T = 298$ K. The narrowest radius of the pore model was used for $r$.

Simulations were carried out in the following way. First, we used the three models having different electrolyte shielding effects to calculate the *I-V* curve of alm-Q7Q18. The narrowest pore radius in each model was changed from 0.3

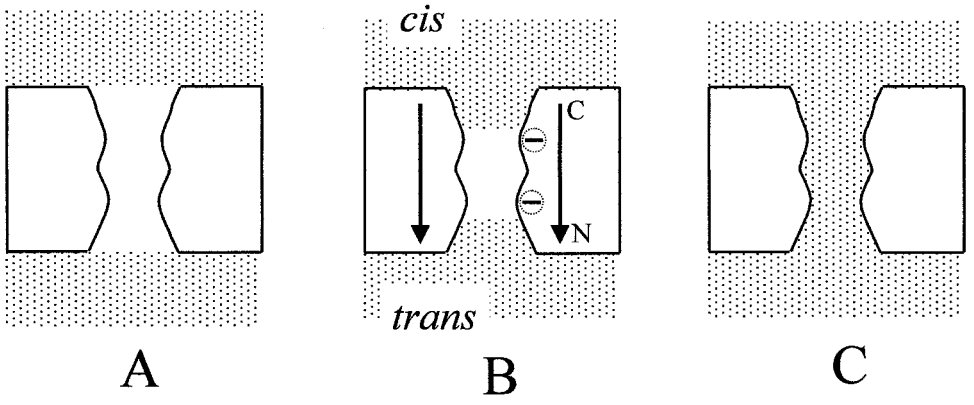


FIGURE 6 Macroscopic pore models used for calculation of energy barriers for ion permeation. Relative permittivity is assumed to be 80 for the aqueous phase and the pore interior and 2 for the membrane and the pore wall. The three models are different only in the ion-exclusion map; electrolytes are fully excluded from the pore interior in model A, penetrate only the pore entrance in model B, and the entire pore in model C. Note that the pore mouth at the *cis* side is wider than that at the *trans* side.

to 0.6 nm by 0.05 nm to obtain a theoretical *I-V* curve close to the observed one. The results are shown in Fig. 6, where the pore radius is 0.55 nm for model A, 0.5 nm for model B, and 0.35 nm for model C. The theoretical *I-V* curve seriously depended on the pore model used, suggesting that electrolyte shielding is an important factor to determine the energy barrier of ion permeation as pointed out by Jordan et al. (1989). Because model B, with $r = 0.5$ nm, provided a better simulation for the *I-V* curve of alm-Q7Q18, we used this model for simulating the *I-V* curves of the other three peptides. The *I-V* curves for alm-Q7E18 and alm-E7Q18 were calculated by varying the total charge of E18 or E7 in a hexameric bundle, the best-fit curves being obtained with total charges of 0.6*e* for E18 and 1.1*e* for E7 (*e* is the

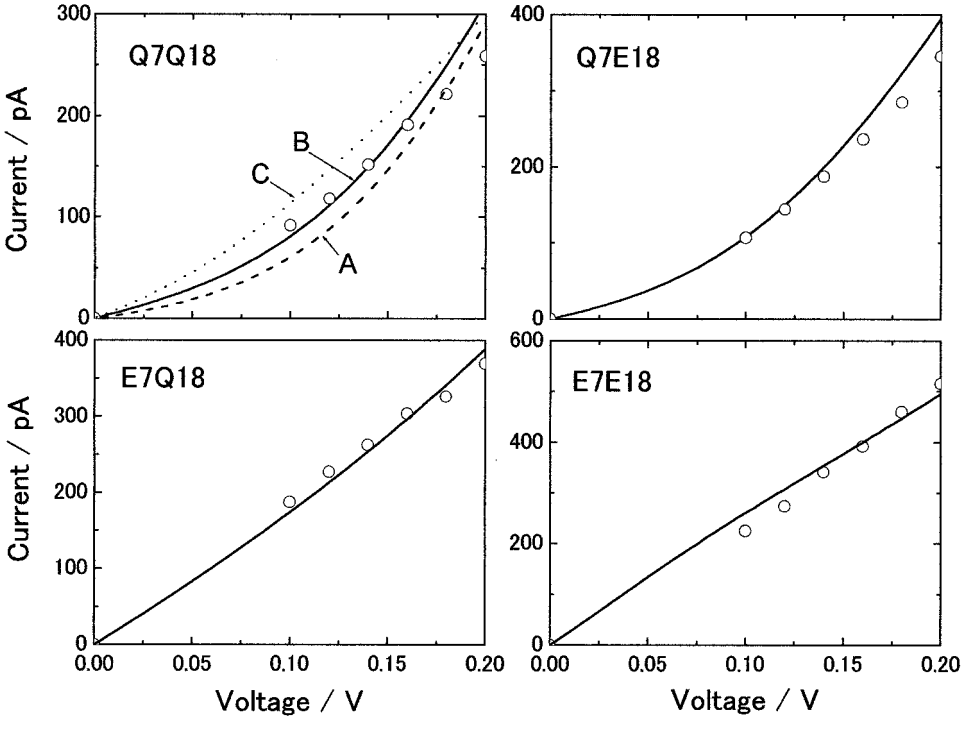


FIGURE 7 Simulation of *I-V* curves of level 2 channels at pH 6.7–6.9. For the alm-Q7Q18 channel, the three pore models shown in Fig. 6 were fitted by adjusting the narrowest pore radius *r*. *Curve A* was calculated using model A with $r = 0.55$ nm; *curve B*, model B with $r = 0.5$ nm; *curve C*, model C with $r = 0.35$ nm. The *I-V* curves for alm-Q7E18, alm-E7Q18, and alm-E7E18 are obtained with model B with $r = 0.5$ nm by adjusting the total charges of E7 and E18. The best-fit values of the total charges were 1.1*e* for E7 and 0.6*e* for E18.

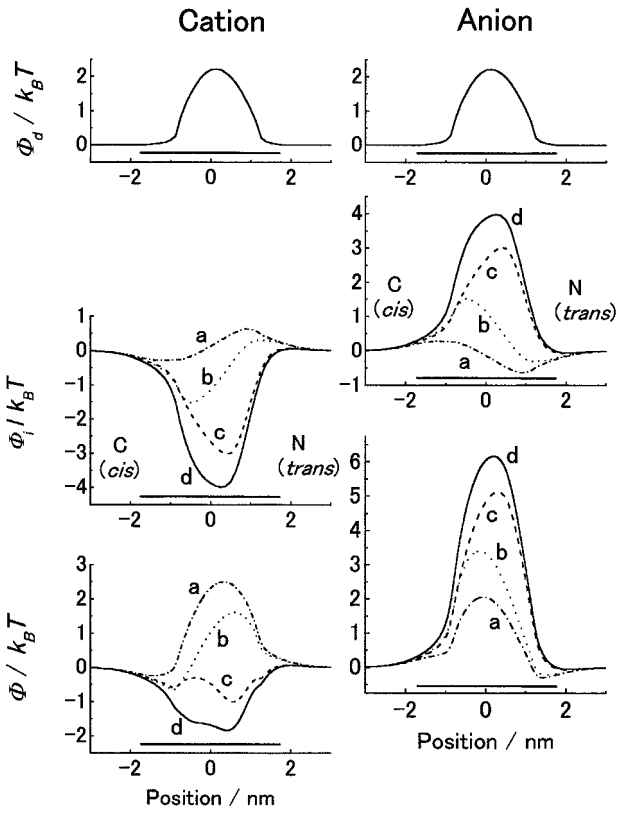


FIGURE 8 Potential energy profiles for a cation and an anion, from which the *I-V* curves (shown in Fig. 7) were calculated. $\Phi_d$, the "desolvation" energy that is the self energy difference of a permeating ion; $\Phi_i$, the "interaction" energy that is due to the interactions of a permeating ion with charges of ionized residues and dipole moments of helix backbones; $\Phi = \Phi_d + \Phi_i$. In $\Phi_i$ and $\Phi$: *curve a*, alm-Q7Q18; *b*, alm-Q7E18; *c*, alm-E7Q18; *d*, alm-E7E18. The horizontal bars indicate the membrane region.

elementary charge) (shown in Fig. 7). Finally, the *I-V* curve of alm-E7E18 was calculated with the same total charges of E7 and E18 that were estimated for alm-Q7E18 and alm-E7Q18 channels. The resulting potential profiles are shown in Fig. 8. These simulations provided a reasonable explanation for the differences in nonlinearity among the observed *I-V* curves, irrespective of the simplified calculations that were based on static potential energy profiles without taking into account interactions between permeating ions. For the more precise simulations, which would be a future issue, we should take into account dynamic interactions of permeating ions with charged residues and multi-ion permeation.

## Cation/anion selectivity

In the determination of ion selectivity of alamethicin channels we cannot use the "reversal potential" method because the channels open only at *cis*-positive voltages and close before reaching the reversal potentials. Hence, the $K^+/Cl^-$ selectivity has been estimated from the single-channel currents in 1 M potassium gluconate (Kgluc) and 1 M *N*-methylglucamine chloride (NmgCl), both buffered with 10 mM HEPES-KOH (pH 7.0). Because of the bulky organic counterions, channel currents through small pores are mainly carried by $K^+$ or $Cl^-$, and thus the channel current ratio $I_{Kgluc}/I_{NmgCl}$ indicates the $K^+/Cl^-$ selectivity. In the calculation of $I_{Kgluc}/I_{NmgCl}$ the assignment of conductance levels is very important. For alm-Q7Q18 and alm-Q7E18, single-channel recordings in 1 M Kgluc and 1 M NmgCl were not so different from each other, and therefore the conductance levels were unambiguously assigned. For alm-E7Q18 and alm-E7E18, however, single-channel recordings were very different between 1 M Kgluc and 1 M NmgCl, and the probabilities of lower conductance levels in 1 M Kgluc were extremely reduced (Fig. 9). This situation made it difficult to identify the conductance levels. Hence, we followed the single-channel conductances by varying the solution composition from 100% NmgCl to 100% Kgluc.

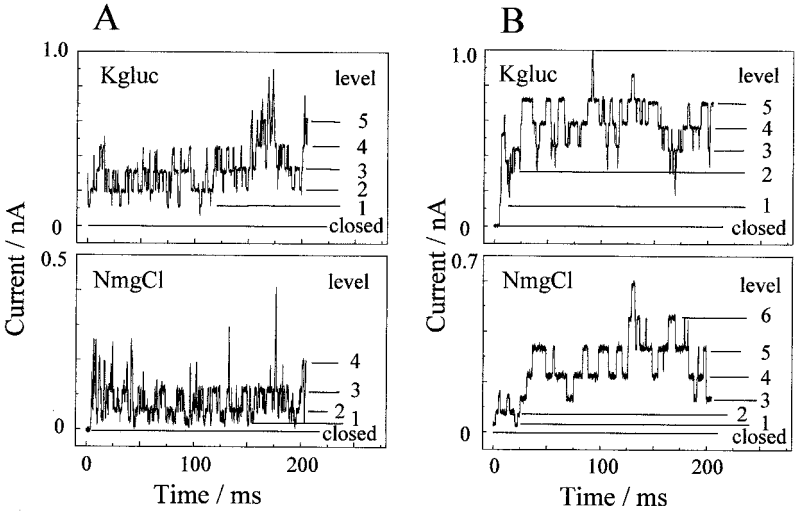


FIGURE 9 Single-channel recordings of (*A*) alm-E7Q18 channels and (*B*) alm-E7E18 channels in 1 M Kgluc (pH 7.0) and 1 M NmgCl (pH 7.0). Applied voltage was 200 mV.

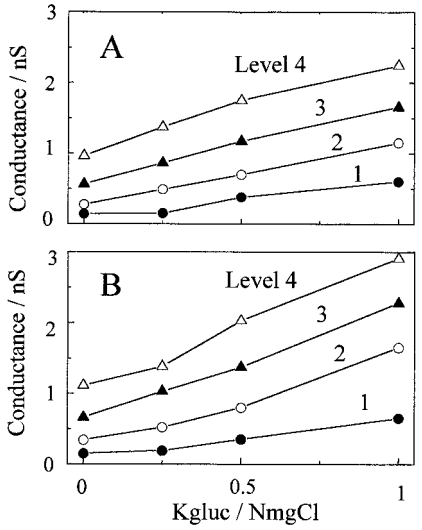


FIGURE 10 Changes in single-channel conductance for (*A*) alm-E7Q18 and (*B*) alm-E7E18 by varying the solution composition from 100% 1 M NmgCl (pH 7.0) to 100% 1 M Kgluc (pH 7.0). Applied voltage was 200 mV.

The results are shown in Fig. 10. The conductance of each level was proportional to the Kgluc/NmgCl ratio, which allowed us to identify the conductance levels unambiguously. Table 2 summarizes mean values of $I_{Kgluc}/I_{NmgCl}$ obtained at 200 mV. Both alm-E7Q18 and alm-E7E18 channels were strongly cation-selective, i.e., the $I_{Kgluc}/I_{NmgCl}$ was 4–5 for level 1 channels, decreasing with increasing conductance-level number. Compared with the peptides with E7 (alm-E7Q18 and E7E18), weak cation selectivity was obtained for the peptides with Q7 (alm-Q7Q18 and alm-Q7E18). These results indicate that negative charges at position 7 strongly enhance the cation selectivity, whereas those at position 18 slightly influence the charge selectivity.

The "current ratio" method usually provides an underestimated value for the permeability ratio that is calculated by the "reversal potential" method. Starostin et al. (1999) determined the $K^+/Cl^-$ selectivity of channels formed by the covalent dimer of alamethicin (Rf50) (di-alm-Q18) and that of its analog with Lys-18 (di-alm-K18) by the two methods. Because the dimers formed long-lasting channels, the entire *I-V* curves of the single channels were obtained by applying fast voltage ramps during their opening, and thus the reversal potentials were measured in asymmetric KCl solutions. The permeability ratio $P_K/P_{Cl}$ of the octamer level channel (level 4) was 2.1 (0.1 M/1.3 M KCl) for di-alm-Q18, and was 0.56 (0.1 M/1.3 M KCl) for di-alm-K18 at pH 6.8. However, the corresponding current ratio $I_K/I_{Cl}$ measured in electrolyte solutions of bulky counterions was 1.1 for di-alm-Q18 and 0.7 for di-alm-K18 at pH 7.0.

Borisenko et al. (2000) demonstrated that di-alm-K18 formed anion-selective, non-selective, and cation-selective channels depending on pH. The $P_{K+}/P_{Cl-}$ was 0.25 at pH below 7 and was 4 at pH above 11. Lear et al. (1997) studied electrostatic effects on charge selectivity with ion channels formed by designed peptides (Ac-$(LSSLLSL)_3$-$CONH_2$). They found that a negatively charged Glu introduced at the N-terminus enhanced the cation selectivity of the channels, and a positively charged Arg at the N-terminus reduced the cation selectivity. It may be concluded from these results and the present results that the charge selectivity can be modified by introducing dissociable residues to channel-forming peptides and by varying pH of membrane-bathing solutions. In particular, charged residues in the pore interior are much more effective than those at the pore mouth.

**TABLE 2 $K^+/Cl^-$ selectivity determined from channel currents measured in 1 M Kgluc and 1 M NmgCl at 200 mV**

| | $I_{Kgluc}/I_{NmgCl}$ | | | |
|---|---|---|---|---|
| Level | alm-Q7Q18 | alm-Q7E18 | alm-E7Q18 | alm-E7E18 |
| 1 | 3.6 | 1.2 | 4* | 5* |
| 2 | 2.4 | 1.5 | 4.2 | 4.8 |
| 3 | 1.6 | 1.6 | 2.9 | 3.5 |
| 4 | 1.4 | 1.5 | 2.3 | 2.6 |
| 5 | — | 1.4 | — | 2.2 |

The values of $I_{Kgluc}/I_{NmgCl}$ were mean values for at least three separate measurements.

*The value included large uncertainty because the probability of the level 1 channel in 1 M Kgluc was very low.

## REFERENCES

Baumann, C., and P. J. Mueller. 1974. A molecular model of membrane excitability. *J. Supramol. Struct.* 2:538–557.

Bertho, J-N., A. Loffet, C. Pinel, F. Reuther, and G. Sennyey. 1991. Amino acid fluorides: their preparation and use in peptide synthesis. *Tetrahedron Lett.* 32:1303–1306.

Bezrukov, S. M., R. P. Rand, I. Vodyanoy, and V. A. Parsegian. 1998. Lipid packing stress and polypeptide aggregation: alamethicin channel probed by proton titration of lipid charge. *Faraday Discuss.* 111: 173–183.

Boheim, G. 1974. Statistical analysis of alamethicin in a lipid membrane. *J. Membr. Biol.* 19:277–303.

Borisenko, V. B., M. S. P. Sansom, and G. A. Woolley. 2000. Protonation of lysine residues inverts cation/anion selectivity in a model channel. *Biophys. J.* 78:1335–1348.

Cafiso, D. S. 1994. Alamethicin: a peptide model for voltage gating and protein membrane interactions. *Annu. Rev. Biophys. Biomol. Struct.* 23:141–165.

Dieckmann, G. R., J. D. Lear, Q. Zhong, M. L. Klein, W. F. DeGrado, and K. A. Sharp. 1999. Exploration of the structural features defining the conduction properties of a synthetic ion channel. *Biophys. J.* 76: 618–630.

Eisenberg, M., J. E. Hall, and C. A. Mead. 1973. The voltage-dependent conductance induced by alamethicin in black lipid membranes. *J. Membr. Biol.* 14:143–176.

Fox, R. O., Jr., and F. M. Richards. 1982. A voltage-gated ion channel model inferred from the crystal structure of alamethicin at 1.5-Å resolution. *Nature.* 300:325–330.

Gordon, L. G. M., and D. A. Haydon. 1975. Potential-dependent conductances in lipid membranes containing alamethicin. *Phil. Trans. R. Soc. Lond. B.* 270:433–447.

Hanke, W., and G. Boheim. 1980. The lowest conductance state of the alamethicin pore. *Biochim. Biophys. Acta.* 596:456–462.

Jordan, P. C., R. J. Bacquet, J. A. McCammon, and P. Tran. 1989. How electrolyte shielding influences the electrical potential in transmembrane ion channels. *Biophys. J.* 55:1041–1052.

Kaduk, C., M. Dathe, and M. Bienert. 1998. Functional modifications of alamethicin ion channels by substitution of glutamine 7, glycine 11 and proline 14. *Biochim. Biophys. Acta.* 1373:137–146.

Keller, S. L., S. M. Bezrukov, S. M. Gruner, M. W. Tate, I. Vodyanoy, and V. A. Parsegian. 1993. Probability of alamethicin conductance states varies with nonlamellar tendency of bilayer phospholipids. *Biophys. J.* 65:23–27.

Koide, N., K. Asami, and T. Fujita. 1997. Ion channels of hypelcins, antibiotic peptides, formed in planar bilayer lipid membranes. *Biochim. Biophys. Acta.* 1326:47–53.

Latorre, R., and O. Alvarez. 1981. Voltage-dependent channels in planar lipid bilayer membranes. *Physiol. Rev.* 61:77–150.

Lear, J. D., J. P. Schneider, P. K. Kienker, and W. F. DeGrado. 1997. Electrostatic effects on ion selectivity and rectification in designed ion channel peptides. *J. Am. Chem. Soc.* 119:3212–3217.

Levitt, D. G. 1999. Modeling of ion channels. *J. Gen. Physiol.* 113: 789–794.

Mak, D. D., and W. W. Webb. 1995. Two classes of alamethicin transmembrane channels: molecular models from single-channel properties. *Biophys. J.* 69:2323–2336.

Matsubara, A., K. Asami, A. Akagi, and N. Nishino. 1996. Ion channels of cyclic template-assembled alamethicins that emulate the pore structure predicted by barrel-stave model. *J. Chem. Soc., Chem. Commun.* 2069–2070.

Molle, G., J.-V. Dugast, G. Spach, and H. Duclohier. 1996. Ion channel stabilization of synthetic alamethicin analog by rings of inter-helix H-bonds. *Biophys. J.* 70:1669–1675.

Montal, M., and P. Mueller. 1972. Formation of bimolecular membranes from monolayers and study of their properties. *Proc. Natl. Acad. Sci. U.S.A.* 69:3561–3566.

Nagaoka, Y., A. Iida, T. Kambara, K. Asami, and T. Fujita. 1996a. Role of Gln-7 in the ion-channel-forming properties of the peptaibol trichosporin-B-Via. *J. Chem. Soc., Chem. Commun.* 1079–1080.

Nagaoka, Y., A. Iida, T. Kambara, K. Asami, E. Tachikawa, and T. Fujita. 1996b. Role of proline residue in the channel-forming and catecholamine-releasing activities of the peptaibol, trichosporin-B-Via. *Biochim. Biophys. Acta.* 1283:31–36.

Parsegian, A. 1969. Energy of an ion crossing a low dielectric membrane: solutions to four relevant electrostatic problems. *Nature.* 221:844–846.

Sansom, M. S. P. 1991. The biophysics of peptide models of ion channels. *Prog. Biophys. Mol. Biol.* 55:139–235.

Sansom, M. S. P. 1993. Structure and function of channel-forming peptaibols. *Q. Rev. Biophys.* 26:365–421.

Sharp, K. A., and B. Honig. 1990. Electrostatic interactions in macromolecules: theory and applications. *Annu. Rev. Biophys. Biophys. Chem.* 19:301–332.

Starostin, A. V., R. Butan, V. Borisenko, D. A. James, H. Wenschuh, M. S. P. Sansom, and G. A. Woolley. 1999. An anion-selective analogue of the channel-forming peptide alamethicin. *Biochemistry.* 38: 6144–6150.

Taylor, R. J., and R. de Levie. 1991. "Reversed" alamethicin conductance in lipid bilayers. *Biophys. J.* 59:873–879.

Tieleman, P. D., H. J. C. Berendsen, and M. S. P. Sansom. 1999. An alamethicin channel in a lipid bilayer: molecular dynamic simulations. *Biophys. J.* 76:1757–1769.

Wenschuh, H., M. Beyermann, H. Haber, J. K. Seydel, E. Krause, M. Bienert, L. A. Carpino, A. El-Faham, and F. Albericio. 1995. Stepwise automated solid phase synthesis of naturally occurring peptaibols using FMOC amino acid fluorides. *J. Org. Chem.* 60:405–410.

Woolley, G. A., and B. A. Wallace. 1992. Model ion channels: gramicidin and alamethicin. *J. Membr. Biol.* 129:109–136.

You, S., S. Peng, L. Lien, J. Breed, M. S. P. Sansom, and G. A. Woolley. 1996. Engineering stabilized ion channels: covalent dimers of alamethicin. *Biochemistry.* 35:6225–6232.